Supplement of Nat. Hazards Earth Syst. Sci., 26, 1417–1433, 2026
https://doi.org/10.5194/nhess-26-1417-2026-supplement

Natural Hazards and Earth System Sciences
Open Access
EGU

Supplement of

Climate and impact attribution of compound flooding induced by tropical cyclone Idai in Mozambique

Doris M. Vertegaal et al.

Correspondence to: Doris M. Vertegaal (doris.vertegaal@deltares.nl)

Supplementary material

S1 Method material

S1.1 SFINCS Basemap

Figure S1 shows the SFINCS model domain with its elevation, in- and -outflow boundaries and output points for timeseries analyses. SFINCS uses the simulated wflow discharge as input for the fluvial flooding, and the D-Flow FM – SnapWave simulated coastal water levels as input for the coastal flooding.

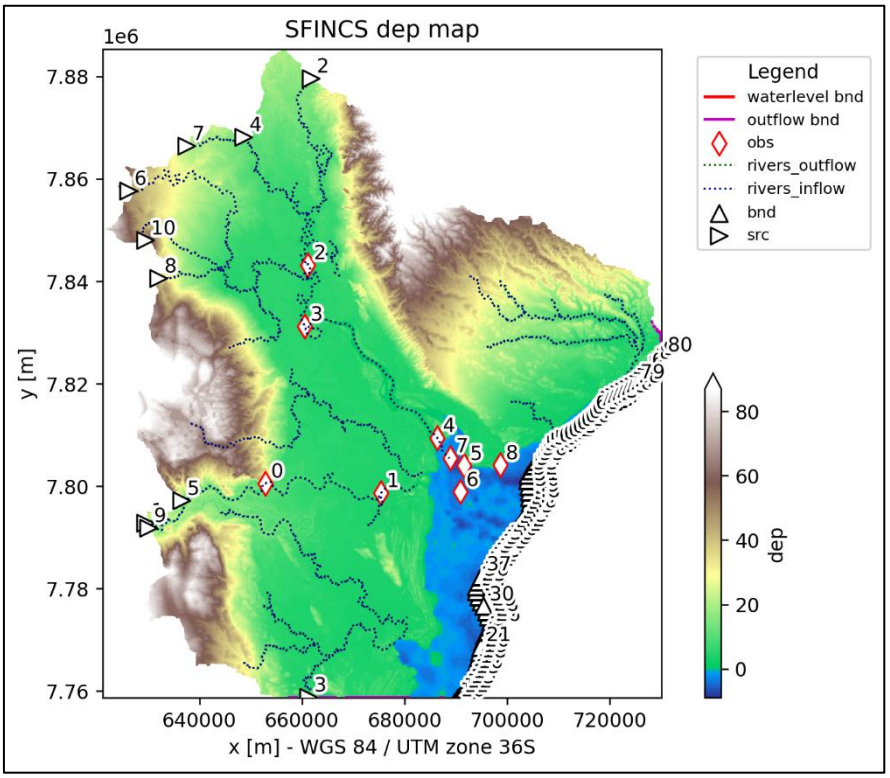

Figure S1: Basemap of the local SFINCS model with the boundary conditions coupling the wflow discharge output (src), water level boundary coupling the D-Flow FM – SnapWave output (bnd), outflow boundary (outflow bnd), rivers, elevation (dep), and the SFINCS output points for timeseries data (obs).

S1.2 Wflow bankfull discharge

Figure S2 shows the estimated return values for extreme discharge in the two largest rivers, the Buzi (Gauge 1) and the Pungwe (Gauge 2), see Figure S4 for gauge locations. We derive the 2-year return period for all gauges (Table S1) by extracting annual maxima from the discharge time series from the 30-year wflow simulation (1989-2019) and fitting a Generalized Extreme

Value (GEV) or Gumbel distribution (a specific case of the GEV distribution with the shape parameter being 0) to the extremes, based on the Akaike Information Criterion goodness-of-fit metric, as implemented in the pyextremes Python package (Bocharov, 2023). The estimated 2-year return period is removed from the wflow simulated discharge of the event (example for the Buzi river in Fig. S3). The 2-year return period represents an approximation of the bankfull river discharge and this relationship is based on semi-empirical relationships (Liu et al., 2024). Due to the lack of river bathymetry data, we remove the bankfull discharge from the discharge boundary conditions for SFINCS and assume that the incoming discharge represents out of banks discharge, thereby removing the need to burn in an (unknown) river conveyance in the digital elevation model. This approach may lead to an under- or overestimation in river discharge input for our SFINCS model simulations.

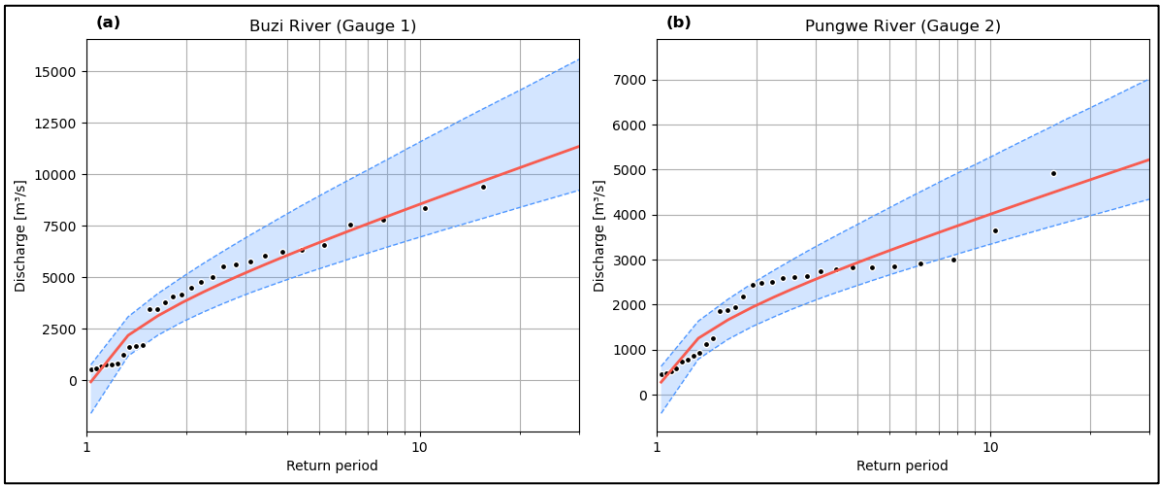

Figure S2: Discharge return levels (m^3/s) obtained for the Buzi (a) and the Pungwe (b) rivers, based on a Gumbel distribution (Bocharov, 2023). The fit obtained is shown in red and confidence interval (5-95%) in blue. The ranked yearly maxima from the 30-year time series (1989-2019) are shown in black.

Table S1: The estimated 2-year return period (bankfull discharge) in m^3/s from the GEV or Gumbel fit (based on the Akaike Information Criterion goodness-of-fit metric) for all discharge boundary points of the SFINCS model domain (see Fig. S4 for locations), together with the upper and lower 95% confidence intervals (CI) in m^3/s.

Gauge ID	Bankfull Discharge (m^3/s)	Lower 95% CI (m^3/s)	Upper 95% CI (m^3/s)
1	3888	2921	5212
2	1992	1566	2515
3	102	72	174
4	179	136	237
5	197	143	272
6	99	70	155

7	30	23	40
8	15	10	27
9	89	62	123
10	11	7	18

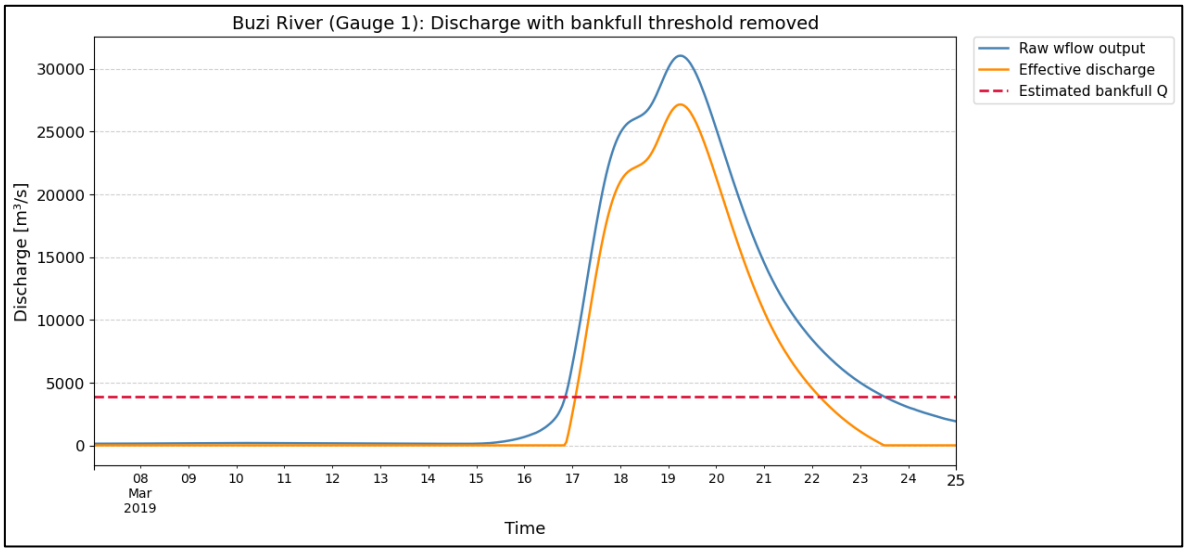

Figure S3: Example of bankfull discharge removal for the Buzi river (Gauge 1) for the period of TC Idai. The estimated 2-year return period (red) is removed from the wflow output (blue) to correct for missing river bathymetry before provided as effective discharge (orange) to SFINCS.

S1.3 Simulated discharge comparison with modelled GloFAS data

The 30-year warm-up simulation of the wflow model is compared with two versions (v4.0 and v3.1) of the Global Flood Awareness System (GloFAS) modelled discharge data (Grimaldi et al., 2023; Joint Research Center and Copernicus Emergency Management Service, 2020; Zsoter et al., 2021), also using the ERA5 reanalysis dataset as meteorological forcing but the hydrological and channel routing model LISFLOOD. The event discharge and 30-year daily timeseries for GloFAS grid cells closest to the wflow gauges for the major Buzi and Pungwe rivers (gauges 1 and 2 in Fig. S4) are compared to the simulated wflow discharge data for these gauges (Figs. S5 and S6). For the period of TC Idai, the summed daily discharges simulated by GloFAS v4.0 (v3.1) differ -19 % (-10 %) and -51 % (29 %) from the summed wflow discharges resampled to a daily time step for the Buzi and the Pungwe, respectively (Table S2). The overestimated discharge could be explained by the higher spatial resolution of our wflow model compared to GloFAS data. For the event, the simulated discharge is in the same order of magnitude as calculated by Eilander et al. (2023a). The agreement between our results and GloFAS for the Buzi river is reasonable (KGE for comparison with GloFAS v4.0 (v3.1) is 0.42 (0.61) for the Buzi river; Fig S6), although also here extremes are generally overestimated, but uncertain for the Pungwe river as GloFAS result varies significantly between data

versions (KGE for comparison with GloFAS v4.0 (v3.1) is 0.09 (0.75) for the Pungwe river; Fig S6) and would require recent local observations to determine the ground truth.

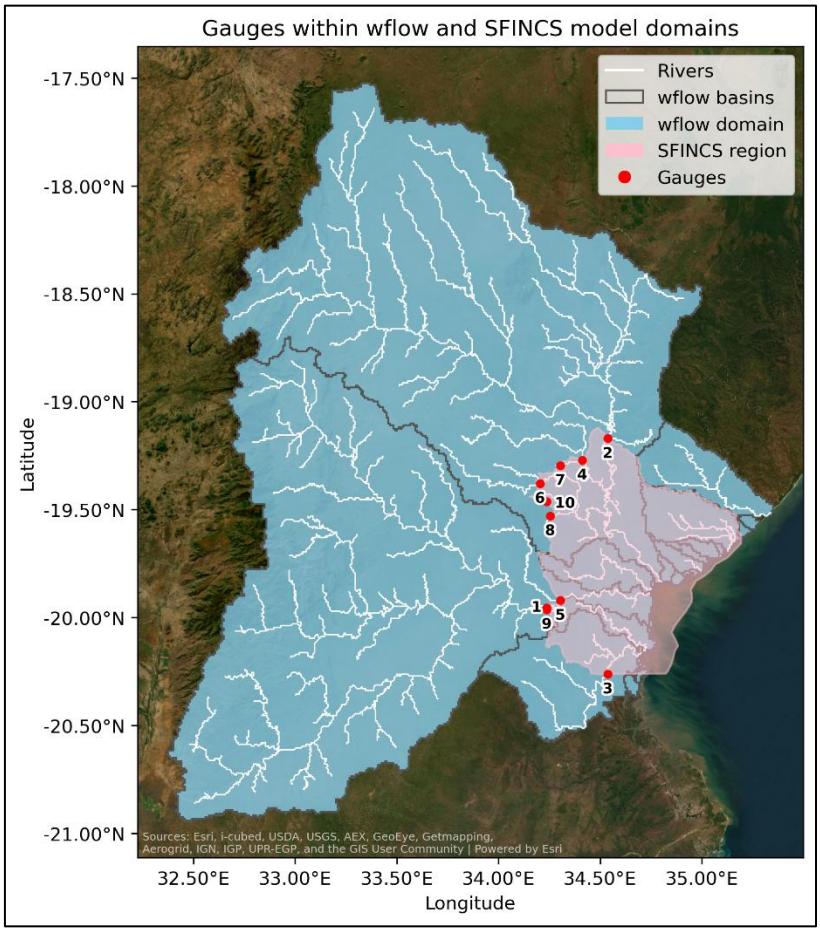

Figure S4: The wflow gauges (red) as output of the hydrological wflow model and input to the SFINCS compound flood model. The major Buzi and Pungwe rivers are modelled as gauge 1 and 2 and have the largest upstream area in the domain. The wflow and SFINCS domains are shown in blue and pink, respectively, as well as the river geometries in white.

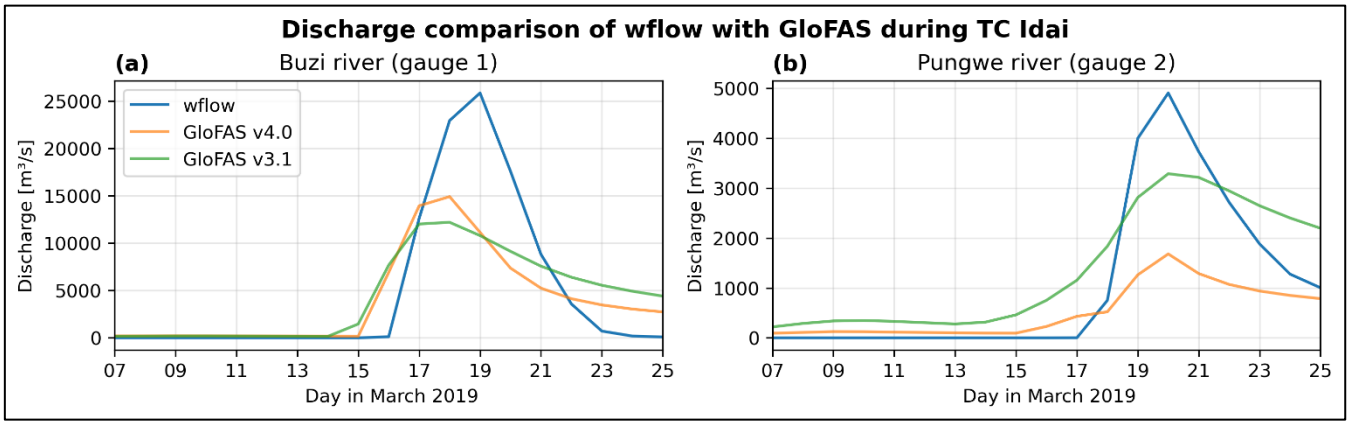

Figure S5: The daily simulated discharge during TC Idai in m^3/s for the Buzi (a) and the Pungwe (b) rivers for the wflow model used in this study (blue), and versions 4.0 (orange) and 3.1 (green) of the globally available GloFAS discharge dataset (wflow is modelled hourly but shown as daily for comparison with GloFAS).

Tabel S2: The total discharge during event of TC Idai (7 to 25 March 2019) for the major Buzi (gauge 1) and Pungwe (gauge 2) rivers as simulated by the wflow model used in this study, and version 4.0 and 3.1 of the globally available GloFAS discharge dataset.

Gauge number	wflow [10^{15} m³]	GloFAS [10^{15} m³]		$\frac{GloFAS - wflow}{wflow}$ [%]	
		v4.0	v3.1	v4.0	v3.1
1	7,99	6,45	7,20	-19	-10
2	1,75	8.65	2,26	-51	29

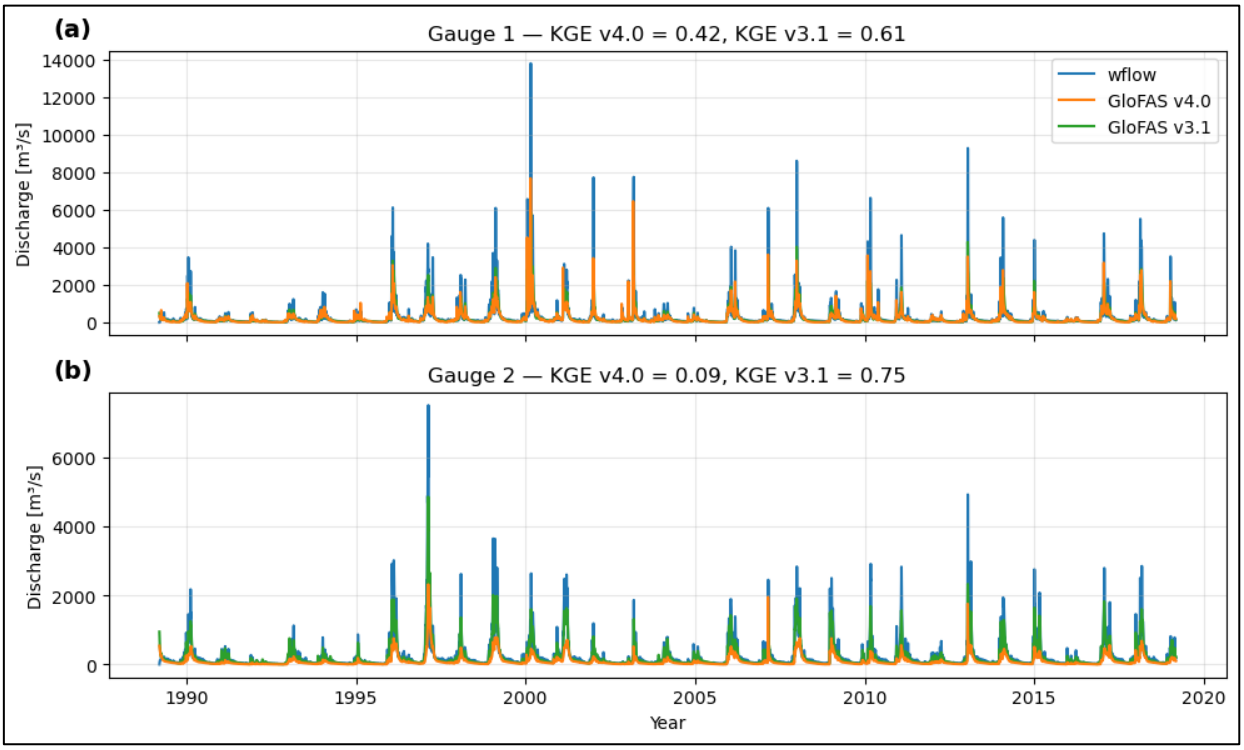

Figure S6: The daily discharge in m^3/s for the Buzi (a) and the Pungwe (b) rivers for the 30-year period prior to the event (1989–2019), for the wflow model used in this study (blue), and version 4.0 (orange) and 3.1 (green) of the globally available GloFAS discharge dataset.

S1.4 SnapWave

Figure S7 shows which SnapWave output points are matched to D-Flow FM output points, with an example of the timeseries for station 62 (panel b). Ideally, the SnapWave coupling would be fully integrated into the SFINCS model of the modelling chain, together with all compound flood drivers simultaneously; however, this was not yet possible at the time of preparation of this paper. Therefore, a nested approach was utilized with 2 different SFINCS simulations.

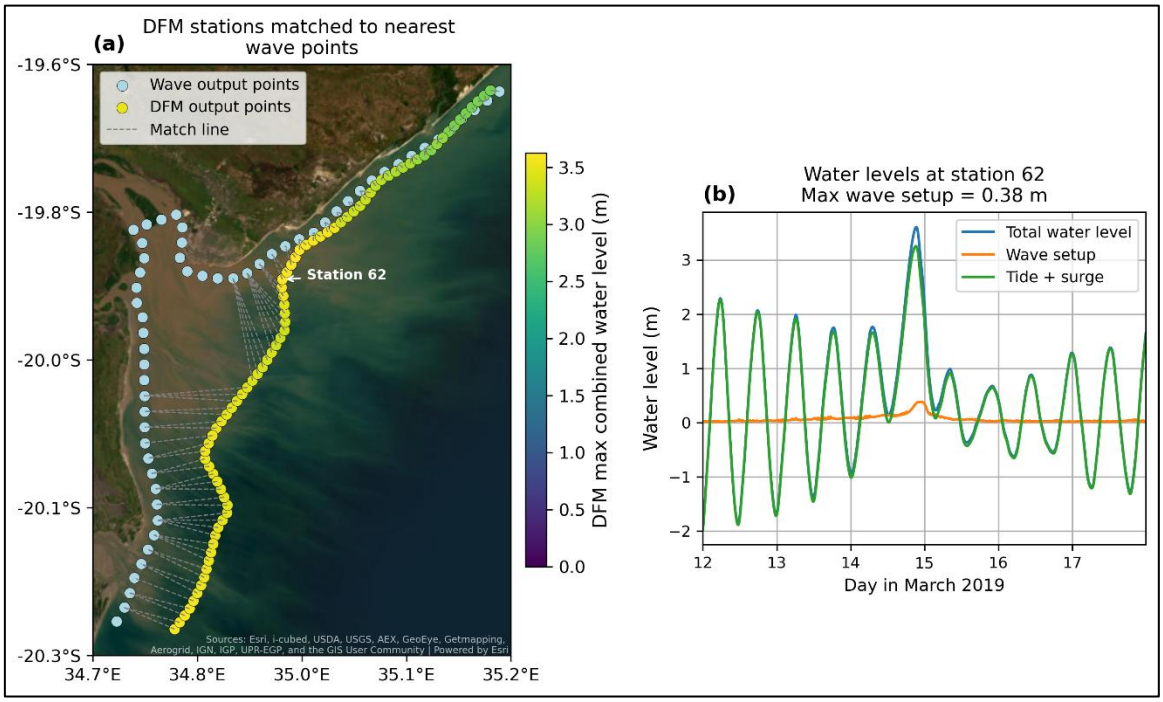

Figure S7: Panel a shows the output points of SnapWave (blue) matched to the D-Flow FM output points, depicted with their maximum water level value (viridis scale), to add the simulated wave setup to the simulated tide and surge. Panel b shows an example of the simulated total water level (blue) after adding wave setup (orange) to tide and surge (green) for the period of 12 to 17 March 2019 at station 62, which is the station closest to Beira.

S1.5 Flood map satellite comparison

The simulated factual flooding from our SFINCS model simulations is compared to the satellite-derived flood extent for TC Idai from UNOSAT (https://unosat.org/products) and CEMS (https://portal.gfm.eodc.eu/; Fig. S8). Several metrics are used to compare our simulated flooding with that derived from the satellite products, based on Eilander et al. (2023). The critical success index (C) is the ratio between the correctly classified instances and the union of both error and correct instances. The hit rate (H) is the proportion of observed flooding that is correctly estimated by the model. The false-alarm ratio (F) is the proportion of modelled flooded area that is not flooded in the observation dataset.

We find a good hit rate when comparing the estimated flooding to both satellite products (> 76%), but a poor false-alarm ratio for the CEMS comparison (60 %). The critical success index is better for the UNOSAT (68 %) than for the CEMS (40 %) comparison. Important to note is the large difference in detected flood extent between the two satellite products, highlighting the lack of "truth". We have more trust in the UNOSAT product, as there is no flooding present in Beira for the CEMS product, even though flooding is documented (e.g. ReliefWeb, 2019). For the region North East of Beira, we underpredict flooding compared to the UNOSAT product but overestimate compared to the CEMS product. This area might be difficult to observe due to the larger elevation gradient with forest transitioning to grass- and cropland (Lisboa et al., 2024).

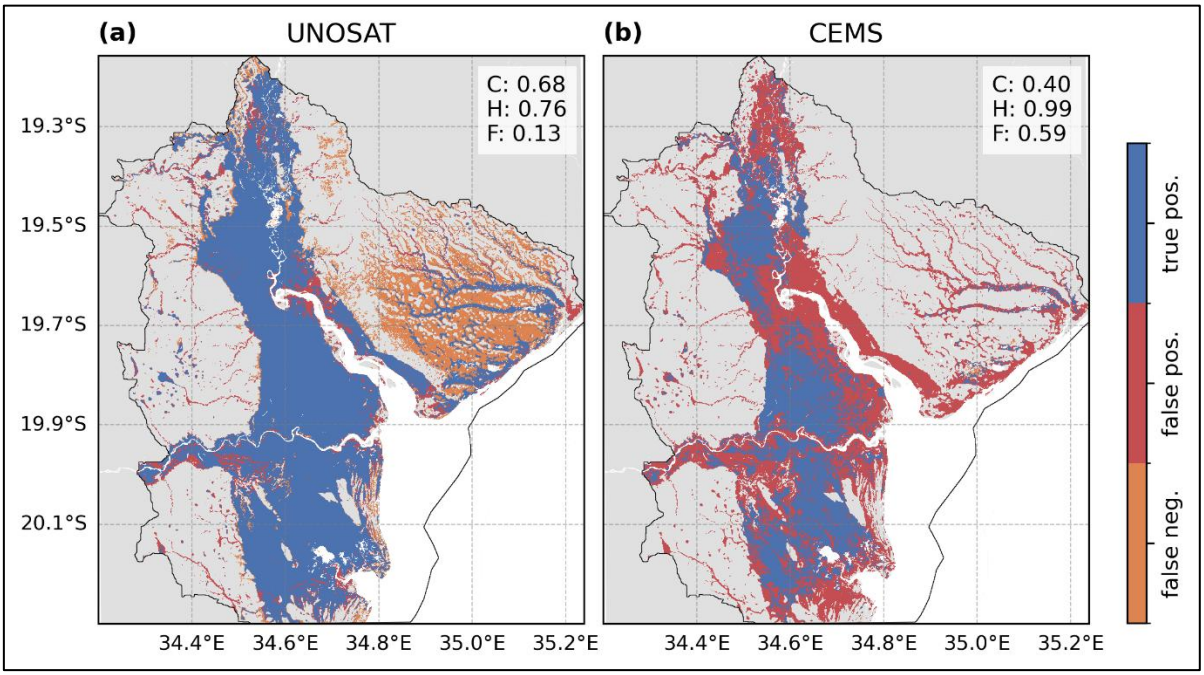

Figure S8: Our factual maximum flood depth simulations compared to satellite observed flood extent of UNOSAT (a) and CEMS (b). The agreement between the model and satellite products is expressed using the critical success index (C), hit rate (H) and false-alarm ratio (F), based on Eilander et al. (2023).

S1.6 Counterfactual forcing

For the counterfactual rainfall scenario, every rainfall value in space and time of the ERA5 reanalysis dataset for the period of the event is multiplied by $1 + \frac{CF_{rain}}{100\,\%}$ to remove the plausible climate trend (where CF_{rain} is -4 %, -8 % or -16 %) of increased rainfall due to climate change from the factual data.

For the counterfactual wind scenario, the maximum sustained wind speed (U_{max}) along the track is adjusted using the counterfactual wind value (CF_{wind}) of -1 %, -5 % or -10 %, following the methodology of Mester et al. (2023):

$$U_{\max\_CF} = U_{max} * 1 + \frac{1}{CF_{wind}} \qquad \text{(S1)}$$

Also the pressure is adjusted accordingly, where the minimum pressure (P_{min}) along the track is increased with the product of the inverse of the counterfactual wind value (CF_{wind}) and the pressure difference between P_{min} and the environmental pressure (P_{env}, Eq. S2). The new wind and pressure values are used to create counterfactual wind and pressure fields for Idai.

$$P_{min\_CF} = P_{min} + -1 * \frac{1}{CF_{wind}} * (P_{env} - P_{min}) \qquad \text{(S2)}$$

For the counterfactual SLR scenario, the SLR is removed from the tidal boundary conditions and initial water level of D-Flow FM using the Python package dfm_tools for pre- and postprocessing of model in- and output files (Veenstra, 2025). The SLR

at all stations along the coast of Mozambique within the D-Flow FM domain are averaged, resulting in a SLR removal of -10 cm for the medium counterfactual scenario. We adjust the medium value by ± 5 cm the low and high counterfactual scenario based on (Strauss et al., 2021). Our SLR estimate is in line with tide gauge observations from the Permanent Service for Mean Sea Level (PSMSL; Holgate et al., 2013; Permanent Service for Mean Sea Level (PSMSL), 2026) at the nearest station with sufficient data, located in Durban, South Africa (analysis not shown). As mentioned in Section 2.1.3, GEBCO v2024 is used to determine the ocean's bathymetry and thereby implicitly the sea level. The ocean depth is referenced to m.s.l., yet the temporal dimension (i.e. reference year) of this mean sea level is not defined. As the development of global bathymetry datasets started in the mid-1990 thanks to the advancement of satellite altimetry (Tozer et al., 2019), we assume that the m.s.l. measured then is the vertical datum still used today. Therefore, we analyse the mean regional SLR from the ISIMIP Hourly Coastal water levels with Counterfactual (HCC) dataset (Treu et al., 2024) for 1990 – 2000 and add the difference between then and medium SLR scenario for 2019 (4 cm; Fig. S10) to the tidal boundary and initial water level of the factual scenario. The difference between 1901 (start of the dataset) and the 1990 – 2000 mean is subtracted from the tidal boundary and initial water level for the different counterfactual scenarios (-1, -6, -11 cm for a SLR scenarios of -5, -10 and -15 cm, respectively). Global bathymetry data inaccuracies can vastly surpass the size of SLR (Tozer et al., 2019) and advancements of local bathymetry data are crucial to accurately estimate the effect of SLR.

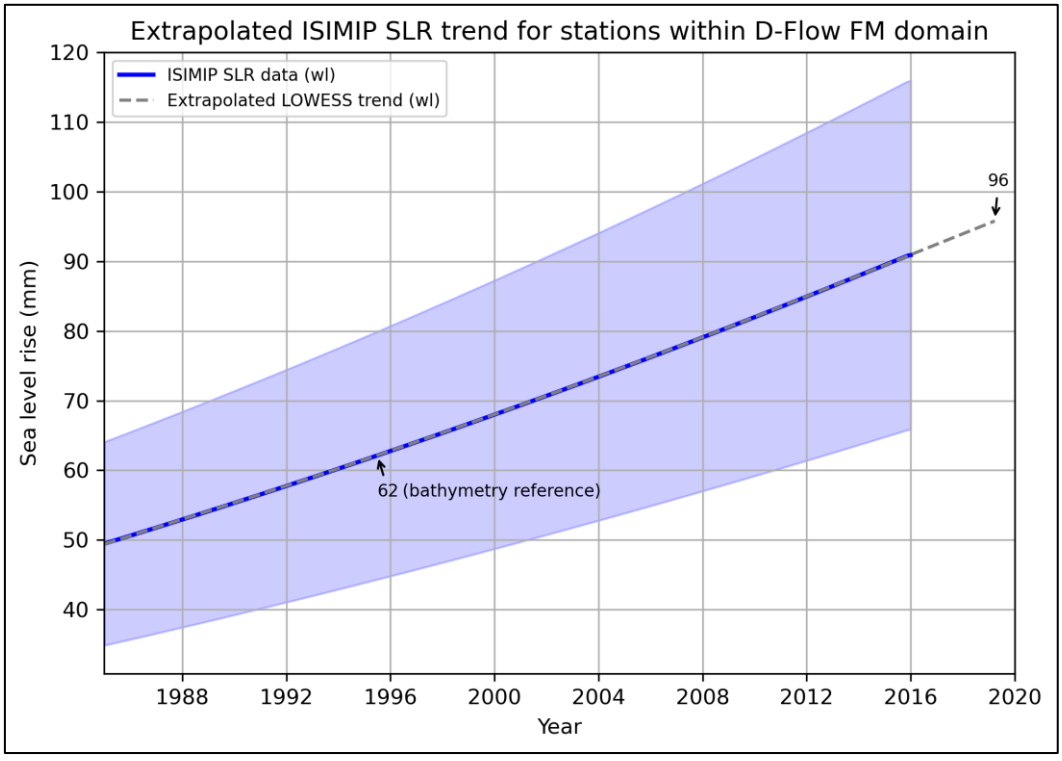

Figure S9: The ISIMIP HCC dataset for 30 years, extrapolated from 2015 to March 2019, when Tropical Cyclone Idai occurred. We use a LOWESS-based extrapolation of the regional average SLR, calculated from stations along the Mozambique coast within

the D-Flow FM domain. To calculate the implicit SLR in the GEBCO bathymetry dataset, we calculate the mean of the SLR between 1990 and 2000, annotated as bathymetry reference.

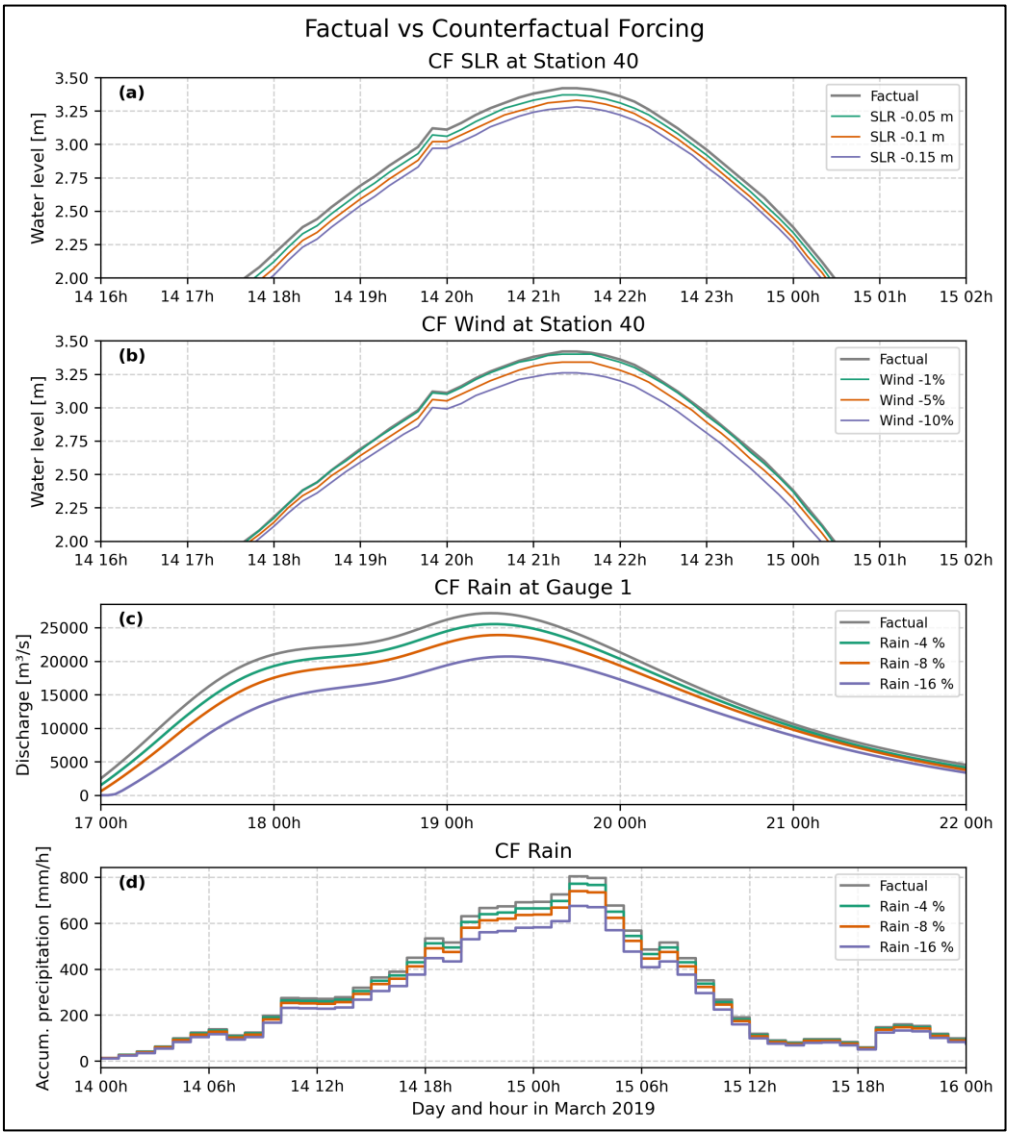

Figure S10: The factual and counterfactual (CF) timeseries data for the change in SLR and wind at a coastal water level boundary point (S40, see Fig S12 for location; panels a and b), the change in rain for two discharge boundary points of the Buzi (G1) and Pungwe (G2) rivers (panel c; for locations see Fig S12), and for change in accumulated rainfall over the SFINCS model domain (panel d). Note the use of different x axis to better capture the timing range of the factual and counterfactual flood driver peaks.

S2 Supplementary result figures

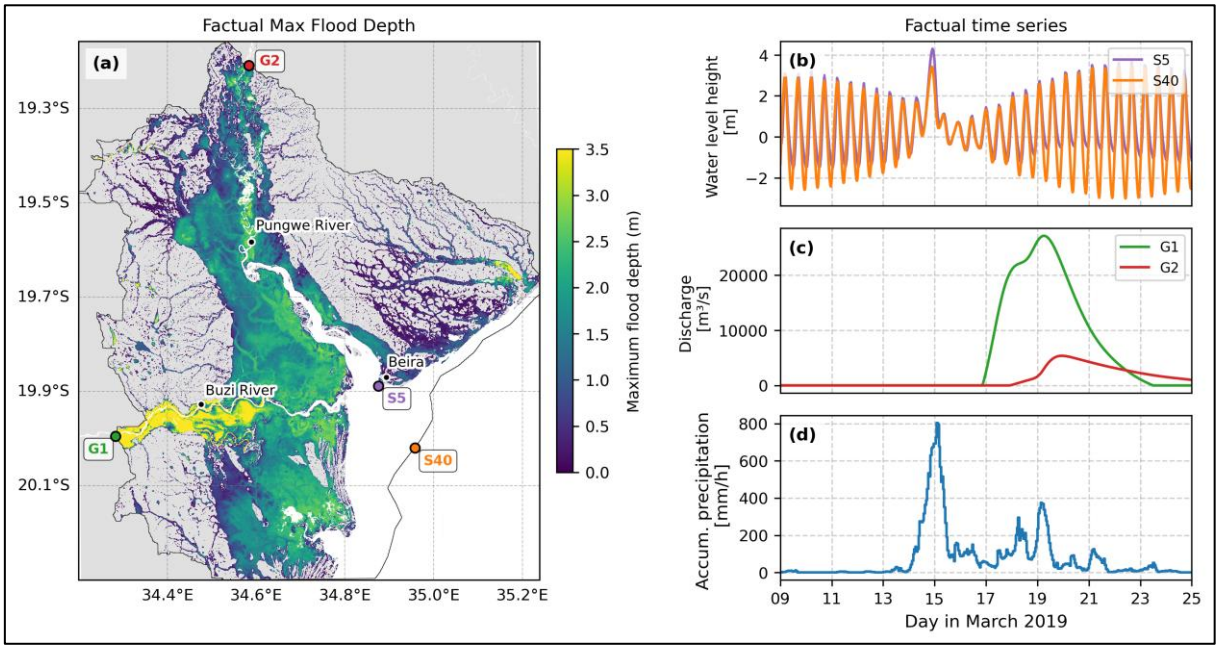

Figure S11: The factual simulated maximum flood depth in meters from TC Idai (a), and the factual forcing over time for coastal water levels at two stations in m (S5 and S40; b), discharge in m^3/s at the Buzi (G1) and Pungwe (G2) rivers (c), and accumulated rainfall over the SFINCS model domain in mm/h from ERA5 (d). The SFINCS model domain is shown in black in panel (a).

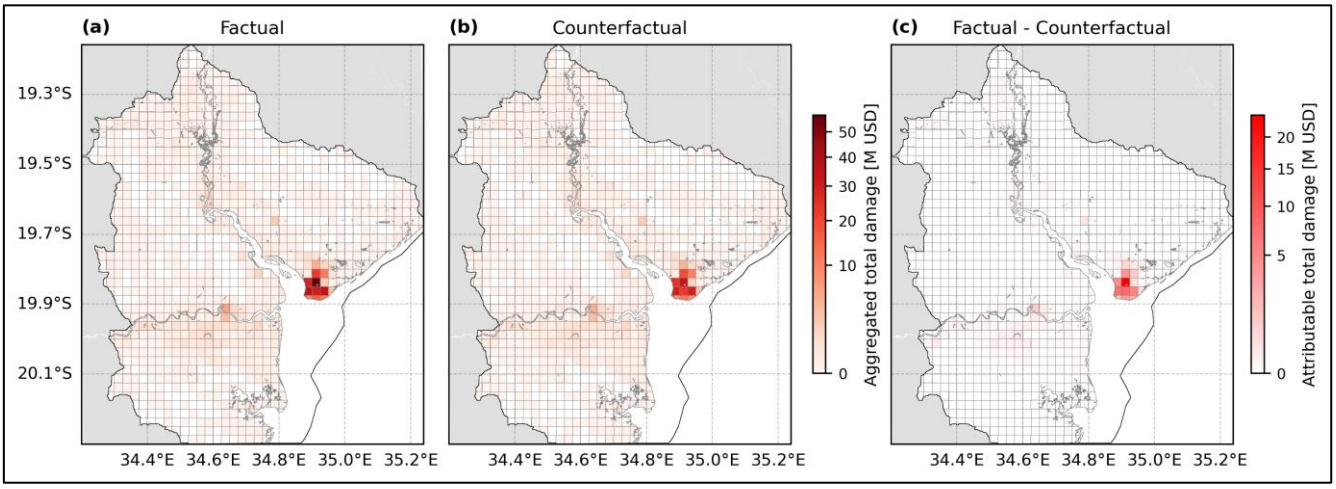

Figure S12: The aggregated (0.025° grid cells) total damage for the factual (a) and medium counterfactual (b) scenarios with all drivers combined, and the absolute difference attributable to climate change (c). The compound flood model (SFINCS) domain is shown in black.

References

Bocharov, G.: pyextremes (Version 2.3.3), https://github.com/georgebv/pyextremes, 2023.

Eilander, D., Couasnon, A., Leijnse, T., Ikeuchi, H., Yamazaki, D., Muis, S., Dullaart, J., Haag, A., Winsemius, H. C., and Ward, P. J.: A globally applicable framework for compound flood hazard modeling, Natural Hazards and Earth System Sciences, 23, 823–846, https://doi.org/10.5194/nhess-23-823-2023, 2023.

Grimaldi, S., Salamon, P., Disperati, J., Zsoter, E., Russo, C., Ramos, A., Carton De Wiart, C., Barnard, C., Hansford, E., Gomes, G., and Prudhomme, C.: River discharge and related forecasted data from the Global Flood Awareness System, https://doi.org/10.24381/cds.a4fdd6b9, 2023.

Holgate, S. J., Matthews, A., Woodworth, P. L., Rickards, L. J., Tamisiea, M. E., Bradshaw, E., Foden, P. R., Gordon, K. M., Jevrejeva, S., and Pugh, J.: New Data Systems and Products at the Permanent Service for Mean Sea Level, J. Coast. Res., 29, 493–504, https://doi.org/10.2112/JCOASTRES-D-12-00175.1, 2013.

Joint Research Center and Copernicus Emergency Management Service: River discharge and related forecasted data from the Global Flood Awareness System, Early Warning Data Store (EWDS), https://doi.org/10.24381/cds.a4fdd6b9, 2020.

Lisboa, S. N., Grinand, C., Betbeder, J., Montfort, F., and Blanc, L.: Disentangling the drivers of deforestation and forest degradation in the Miombo landscape: A case study from Mozambique, International Journal of Applied Earth Observation and Geoinformation, 130, 103904, https://doi.org/10.1016/j.jag.2024.103904, 2024.

Liu, Y., Wortmann, M., Hawker, L., Neal, J., Yin, J., Santos, M. S., Anderson, B., Boothroyd, R., Nicholas, A., Smith, G. S., Ashworth, P., Cloke, H., Gebrechorkos, S., Leyland, J., Zhang, B., Vahidi, E., Griffith, H., Delorme, P., McLelland, S., Parsons, D., Darby, S., and Slater, L.: Global Estimation of River Bankfull Discharge Reveals Distinct Flood Recurrences Across Different Climate Zones, https://doi.org/10.21203/RS.3.RS-5185659/V1, 2024.

Mester, B., Vogt, T., Bryant, S., Otto, C., Frieler, K., and Schewe, J.: Human displacements from Tropical Cyclone Idai attributable to climate change, Hazards Earth Syst. Sci, 23, 3467–3485, https://doi.org/10.5194/nhess-23-3467-2023, 2023.

Permanent Service for Mean Sea Level (PSMSL): Tide Gauge Data, 2026.

ReliefWeb: Mozambique: Cyclone Idai & Floods Situation Report No. 2 (as of 3 April 2019) - Mozambique | ReliefWeb, 2019.

Strauss, B. H., Orton, P. M., Bittermann, K., Buchanan, M. K., Gilford, D. M., Kopp, R. E., Kulp, S., Massey, C., Moel, H. de, and Vinogradov, S.: Economic damages from Hurricane Sandy attributable to sea level rise caused by anthropogenic climate change, Nat. Commun., 12, 2720, https://doi.org/10.1038/s41467-021-22838-1, 2021.

Tozer, B., Sandwell, D. T., Smith, W. H. F., Olson, C., Beale, J. R., and Wessel, P.: Global Bathymetry and Topography at 15 Arc Sec: SRTM15+, Earth and Space Science, 6, 1847–1864, https://doi.org/10.1029/2019EA000658, 2019.

Treu, S., Muis, S., Dangendorf, S., Wahl, T., Oelsmann, J., Heinicke, S., Frieler, K., and Mengel, M.: Reconstruction of hourly coastal water levels and counterfactuals without sea level rise for impact attribution, Earth Syst. Sci. Data, 16, 1121–1136, https://doi.org/10.5194/ESSD-16-1121-2024, 2024.

Veenstra, J.: dfm_tools: A Python package for pre- and postprocessing D-FlowFM model input and output files (v0.35.0), Zenodo, https://doi.org/10.5281/zenodo.14901200, 2025.

Zsoter, E., Harrigan, S., Barnard, C., Wetterhall, F., Ferrario, I., Mazzetti, C., Alfieri, L., Salamon, P., and Prudhomme, C.: River discharge and related forecasted data from the Global Flood Awareness System, https://doi.org/10.24381/cds.a4fdd6b9, 2021.